

# Perovskite/Organic Hybrid White Electroluminescent Devices with Stable Spectrum and Extended Operating Lifetime

Denghui Liu, Xinyan Liu, Yiyang Gan, Zhe Liu, Guanwei Sun, Chenyang Shen, Xiaomei Peng, Weidong Qiu, Deli Li, Zhisheng Zhou, Zhenchao Li, Hin-Lap Yip, and Shi-Jian Su\*

Cite This: *ACS Energy Lett.* 2022, 7, 523–532

Read Online

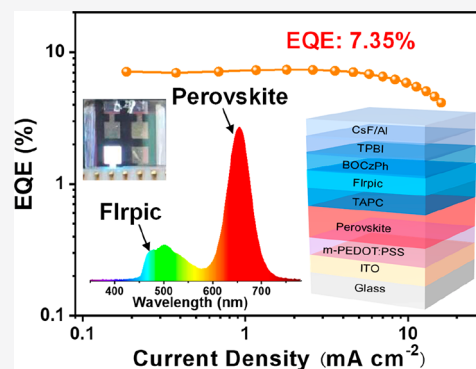
ACCESS |

Metrics & More

Article Recommendations

Supporting Information

**ABSTRACT:** We demonstrate a kind of perovskite/organic hybrid white electroluminescent device, where an ultrathin doping-free organic phosphorescent interlayer is embedded between a p-type hole transport layer and a n-type electron transport layer to give an organic p–i–n heterojunction unit, which is superimposed layer by layer onto a quasi-two-dimensional perovskite layer. The unique carrier transport character of the p-type hole transport layer leads to a broad carrier recombination region approaching the p–i–n heterojunction unit. As a result, pure-red emission from the perovskite layer and sky-blue emission from the organic p–i–n heterojunction were simultaneously achieved to generate white emission with a peak external quantum efficiency of 7.35%, Commission Internationale de L'Éclairage coordinates of (0.424, 0.363), and a low correlated color temperature of 2868 K. More importantly, excellent spectral stability and a greatly enhanced operating lifetime (10-fold longer than those of perovskite-only LEDs) are simultaneously achieved, providing a new path for the development of high-performance white LEDs.



Metal halide perovskites have attracted widespread attention for the next-generation display and solid-state lighting technology due to their advantageous optoelectronic properties, such as high photoluminescence quantum yield (PLQY), high carrier mobility, widely tunable band gap, and low-cost solution processing.<sup>1–5</sup> After the rapid progress in the past few years, the recorded maximum external quantum efficiencies (EQE<sub>max</sub>) of green,<sup>6,7</sup> red,<sup>8</sup> and near-infrared<sup>9</sup> perovskite light-emitting diodes (LEDs) have surpassed 20%, and decent EQEs of over 12% have been realized for blue perovskite LEDs.<sup>10–12</sup>

However, the development of white perovskite LEDs still lags far behind that of their monochromatic LEDs, and only a few perovskite-based white electroluminescent devices have been reported (Table S3),<sup>13–24</sup> possibly limited by the lack of efficient and stable blue perovskite LEDs or the rapid ion exchange reaction between the halogen components of different color perovskites. Efficient white LEDs can be readily achieved by coating perovskite emitters on commercial inorganic LED chips.<sup>25</sup> Some two-dimensional lead-based perovskites<sup>26</sup> and lead-free halide double perovskites<sup>27</sup> taking advantage of broad-band white photoluminescence (PL) from self-trapped excitons have also been developed as emitters in white LEDs, while poor charge-carrier injection and transport

of those materials limit their practical application in electroluminescent (EL) devices, even though strong white PL can be observed. Attempts have been made to create perovskite-based white electroluminescent devices; a series of rare-earth-ion-doped perovskites<sup>20</sup> and heterophase lead halide perovskites<sup>22,24</sup> have been used for fabricating single-emitting-layer white perovskite LEDs whose maximum EQE has reached 6.5%. Nevertheless, the poor EL spectral stability of these devices under different applied biases hardly satisfy the criteria for high-quality lighting. In addition, different-color perovskites with high PLQYs blended with organics,<sup>16,21</sup> polymers,<sup>14</sup> or oligomers<sup>13</sup> were also used to fabricate perovskite/organic hybrid white electroluminescent devices. However, the decreased intermolecular distance increases the unwanted energy transfer (ET), leading to the quenching of blue emission and consequently unsatisfactory white light gen-

Received: December 2, 2021

Accepted: December 28, 2021

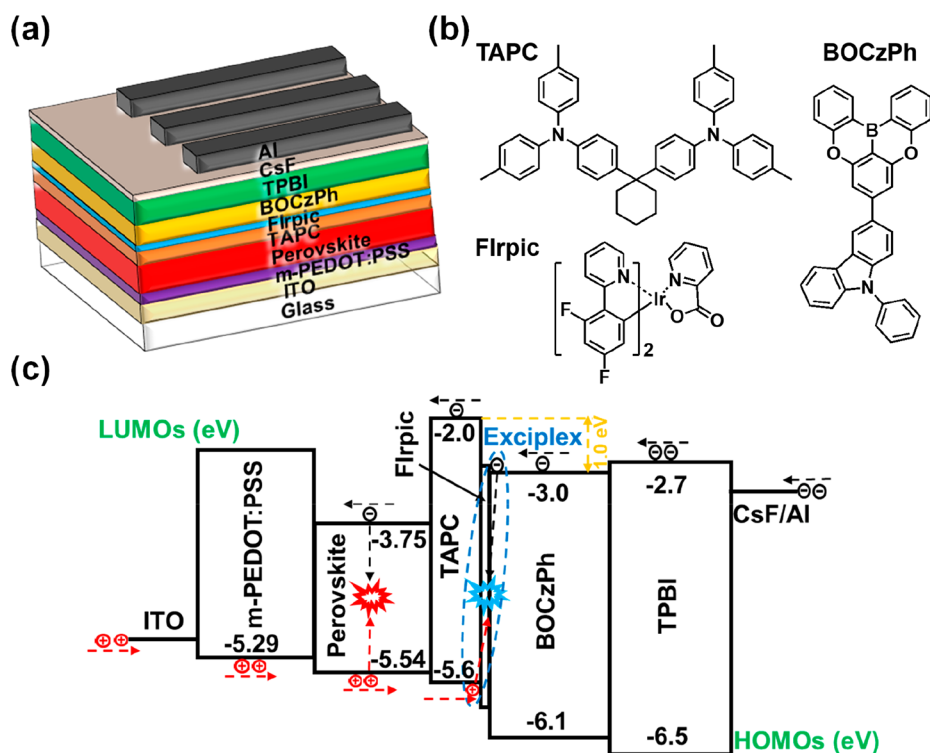


**Figure 1.** (a) Schematic description of the device structure of the perovskite/organic hybrid white LEDs. (b) Molecular structures of the materials used in the organic p–i–n heterojunction. (c) Energy diagram for the device configuration.

eration. Then, bilayer<sup>17</sup> or tandem configurations<sup>15</sup> were employed to suppress the ET process. As a typical example, a cyan perovskite quantum dot was combined with a red two-dimensional (2D) perovskite film and further separated by a well-designed organic interlayer.<sup>15</sup> However, a sophisticated architecture and a complicated process are required for the device preparation, impeding the adaptation of these processing approaches. Soon thereafter, to further simplify the processing route, a single-step antisolvent-assisted spin-coating technology that enables the loading of the red organic compound on a blue-emitting perovskite was proposed.<sup>19</sup> The ET process was effectively suppressed, and the peak EQE was improved to 1.3%; however, the device efficiency and stability were largely limited by the blue perovskites.

Hybridization of red perovskites and blue phosphorescence or thermally activated delayed fluorescence materials might be a more attractive strategy, for which both organics are capable of harvesting singlet and triplet excitons to achieve 100% exciton utilization.<sup>28,29</sup> Unfortunately, perovskite precursors are usually only soluble in a few polar solvents, and the formation of polycrystalline perovskite films needs to undergo an *in situ* self-assembly process. However, organic materials are generally dissolved in nonpolar solvents for spin coating or thermally evaporated under vacuum, which makes the integration of organic/inorganic hybrid emitters into an electroluminescent device challenging. Thus, on consideration of the energy relationship and incompatible processing method, multiple-emission-layer (EML) structures based on red perovskites and blue organics are more suitable to achieve perovskite/organic hybrid white LEDs. When carriers are injected into the device, the red-emitting perovskite with a narrow band gap has the priority to capture carriers, leading to the exciton recombination center being confined in the perovskite layer and only red emission being observed. An

ultrathin red perovskite film might be desirable to reduce the unwanted trap effect; however, it is very challenging to fabricate defect-free and smooth perovskite films below 50 nm. Together with the tremendous difference in carrier mobility between the perovskite film and the organic functional layer, engineering the carrier recombination zone for efficient perovskite/organic hybrid white LEDs is formidable. Thereby, it is urgent to come up with new strategies to eliminate the current dilemma.

Herein, we put forward a facile and efficient approach to realize perovskite/organic hybrid white LEDs by using a pure-red perovskite and a sky-blue organic p–i–n heterojunction as emissive layers. The organic p–i–n heterojunction includes the p-type hole transport layer 4,4'-cyclohexyldienebis[*N,N*-bis(*p*-tolyl)aniline] (p-HTL, TAPC), the embedded ultrathin doping-free organic phosphorescent interlayer iridium(III) bis(3,5-difluoro-2-(2-pyridyl)phenyl(2-carboxypyridyl) (interlayer, Flrpic), and the n-type electron transport layer 3-(5,9-dioxa-13b-boranaphtho[3,2,1-*d,e*]anthracen-7-yl)-9-phenyl-9*H*-carbazole (n-ETL, BOCzPh) (Scheme S1 in the Supporting Information), which are sequentially superimposed onto the perovskite layer via a vacuum deposition technology without the need for a complicated coevaporation process. The p–i–n heterojunction<sup>30–33</sup> with sky-blue emission is introduced as a compensation for the pure-red emitting perovskite, and the unique carrier transport character of the p-HTL in the device leads to a broad carrier recombination region approaching the p–i–n heterojunction unit. As a result, the light emissions from the red perovskite and the blue organic p–i–n heterojunction were simultaneously achieved to generate white emission with a peak EQE of 7.35%, Commission Internationale de L'Éclairage (CIE) coordinates of (0.424, 0.363), and low correlated color temperature (CCT) of 2868 K. In addition, the system also exhibits stable

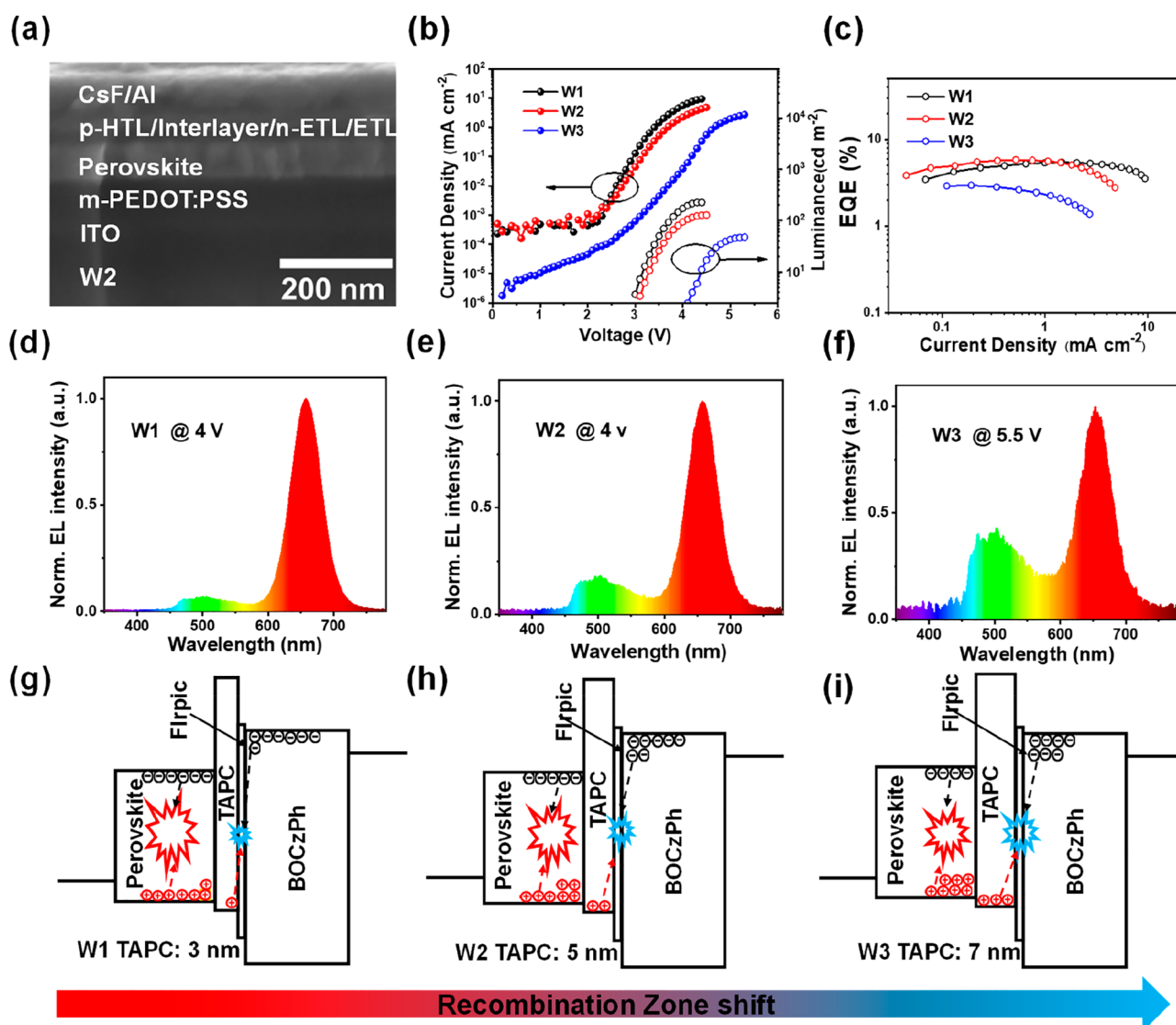


Figure 2. (a) Cross-sectional SEM image of device W2. (b) Current density–voltage–luminance ( $J$ - $V$ - $L$ ) and (c) external quantum efficiency–current density (EQE- $J$ ) characteristics of devices W1–W3. EL spectra of devices (d) W1 and (e) W2 at 4 V and (f) W3 at 5.5 V, where the turn-on voltage of device W3 improves to 4.0 V and its maximum brightness is only 48  $\text{cd m}^{-2}$ . Schematic descriptions of the working mechanisms of devices (g) W1, (h) W2, and (i) W3.

EL spectra under different operating voltages as well as greatly enhanced operating stability (10-fold longer than those of pure-red perovskite LEDs). Advances in the design of more efficient and stable perovskites or organics should further improve the device performance in the future.

Figure 1a depicts the conceptual configuration of the perovskite/organic hybrid white electroluminescent device, where an ultrathin doping-free organic phosphorescent interlayer (Flrpic) is sandwiched between p-HTL (TAPC) and n-ETL (BOCzPh) to give a sky-blue-emitting organic p–i–n heterojunction unit (the molecular structures are shown in Figure 1b), which is deposited layer by layer atop of the pure-red Zn–Pb quasi-2D perovskite film (Note S1 and Figures S1–S5 in the Supporting Information) as coemission layers. In addition, m-PEDOT:PSS is PEDOT:PSS (Al 4083) modified by PSS-Na to achieve an increased work function and better matched energy alignment for hole injection and electron blocking (Figure S1a), TPBI is used as the electron transport layer, and ITO and CsF/Al are used as the anode and cathode,

respectively. The detailed fabrication process of the devices is given in Experimental Section.

The design principle of the device structure is based on the following three considerations and schematically illustrated in Figure 1c. (i) p-HTL is inserted between the perovskite layer and the organic phosphorescent interlayer to increase the intermolecular spatial distance to suppress the ET process, because it is indispensable to get sufficient blue component in white emission. (ii) The modulation of the exciton recombination region is essential for the coemission from the perovskite layer and the organic light-emitting unit, which can be regulated by the insertion of p-HTL. Due to the large electron injection barrier (1.0 eV) existing in the LUMO energy levels of p-HTL and n-ETL, in theory, the electrons passing through the p-HTL to reach the perovskite layer are forbidden. Nevertheless, when the thickness of p-HTL is tuned, electrons can be transported from p-HTL to the perovskite layer by a tunneling effect. As a result, the unique restrictive effect of electron transport leads to fewer electrons reaching the narrow-band-gap perovskite layer to be trapped.



The occurrence of more holes than electrons in the perovskite layer will allow uncaptured holes to pass through the nearly barrier free TAPC layer, and they further encounter the extra electrons accumulated at the interlayer to form excitons, which are then utilized by the organic phosphorescent emitter to give a blue component in white emission. (iii) An ultrathin phosphorescent interlayer is sandwiched by the organic p–n heterojunction to utilize both singlet and triplet excitons for efficient blue light emission. An exciplex can be formed at the interface of the chosen p–n heterojunction (Note S2 and Figures S6 and S7 in the Supporting Information), which can serve as a high-triplet-energy host to sensitize the ultrathin organic phosphorescent interlayer (Note S3 and Figures S8–S10 in the Supporting Information).<sup>34</sup>

Perovskite/organic hybrid white LEDs were fabricated with a device structure of ITO/m-PEDOT:PSS (30 nm)/perovskite (50 nm)/TAPC ( $x$  nm)/Flrpic (1 nm)/BOCzPh (20 nm)/TPBI (30 nm)/CsF (1.2 nm)/Al (120 nm). The thickness of TAPC was tuned from 3 to 5 and 7 nm, corresponding to devices W1–W3, respectively. According to the cross-sectional scanning electronic microscope (SEM) pattern of device W2 (Figure 2a), the thickness of the perovskite layer is approximately 50 nm. As anticipated, the blue and red emission peaks in EL spectra are consistent with their monochromatic devices (Figures S4a and S8a), and white electroluminescence was successfully achieved for devices W2 and W3 with a dominant red emission from the perovskite layer (Figure 2d–f). Interestingly, the intensity of blue light emission from the organic p–i–n heterojunction is gradually enhanced with increased TAPC thickness, corresponding to the trend of CIE coordinate change shown in Figure S11. In addition, charge-carrier injection is simultaneously suppressed with an increase in TAPC thickness from 3 to 7 nm. This in return induces an increased turn-on voltage from 2.9 to 4.0 V (Figure 2b), which can be ascribed to the enhanced confinement for electron transport to the perovskite layer. More importantly, a maximum EQE of 6.16% and a brightness of 148  $\text{cd m}^{-2}$  are achieved for device W2 with CIE coordinates of (0.456, 0.362) and a CCT value of 2348 K. Although a better white emission was obtained when 7 nm TAPC was used, only a peak EQE of 2.96% and a brightness of 48  $\text{cd m}^{-2}$  were achieved for device W3 (Figure 2c and Table 1).

For device W1, nearly only red emission from perovskite can be observed, indicating that the thickness of TAPC is too thin to effectively confine electrons. At the same driving voltage, most of the holes participate in the radiative transition process of the perovskite layer, and only a few uncaptured holes can

pass through the TAPC layer and then encounter electrons to generate excitons for blue emission from the organic phosphorescent emitter. With an increasing thickness of TAPC, the hole transport will not be affected; however, electrons are harder to transport into the perovskite layer, leading to the exciton recombination zone moving to the direction of the cathode. Thus, fewer carrier pairs are trapped in the perovskite layer for reduced red emission intensity, and more uncaptured holes participate in the electroluminescence process demonstrated above for enhanced blue emission, as in the schematic description shown in Figure 2g–i.

Unfortunately, the peak brightness of these perovskite/organic hybrid white LEDs is significantly lower than those of their corresponding monochromatic devices, i.e., R1 and B2 (Note S4 and , Table S2 in the Supporting Information). Thus, we have sought to further improve the device performance through finely altering the thickness of the perovskite film in an architecture of ITO/m-PEDOT:PSS (30 nm)/perovskite (50, 40, or 30 nm)/TAPC (5 nm)/Flrpic (1 nm)/BOCzPh (20 nm)/TPBI (30 nm)/CsF (1.2 nm)/Al (120 nm); the corresponding devices are labeled W2, W4 and W5, respectively (Note S5 and Figures S12–S16 in the Supporting Information). As a result, it is surprising that a maximum EQE of 7.35% and a brightness of 764  $\text{cd m}^{-2}$  can be achieved for device W4 (Table 1), with a CCT value of 2868 K and CIE coordinates of (0.424, 0.363). In comparison with device W2, the significant improvement in the peak EQE and brightness might be attributed to three aspects. (i) In device W2, most of the holes are captured in the perovskite layer and cannot pass through the TAPC layer; however, the excessive electrons accumulate in the organic phosphorescent interlayer, causing unbalanced charge carriers at the p–n heterojunction interface. However, for device W4, the higher hole transport property in the thinner perovskite layer would introduce more holes passing through the TAPC layer, leading to a relatively more balanced charge-carrier recombination in the p–i–n heterojunction unit and thus improved device performance. (ii) More photons emitted from the blue p–i–n heterojunction unit can be extracted through the thinner perovskite layer. (iii) There is a weakened perovskite parasitic absorption loss, evidenced by the obviously reduced red PL emission in thinner perovskite films on excitation by incident blue light (485 nm) with the same intensity (Figure S17). In addition, a detailed optical simulation was performed for red perovskite LEDs (devices R1–R3) to indirectly prove the higher exciton utilization efficiency in device W4. The detailed simulation parameters and process are shown in Figure S18 and Note S6 in the Supporting Information. Figure S18 illustrates the relative average contribution of photon distribution: i.e., the distributed quantum efficiency of all channels dependent on the ETL thickness. At an ETL thickness of 30 nm, a higher theoretical maximum outcoupling efficiency of 17.7% can be predicted for device R2 (40 nm perovskite EML) in comparison with device R1 (50 nm perovskite EML, 15.3%), indicating that more generated photons from the perovskite layer can be extracted from the device. Moreover, the absorption loss in device R2 is predicted to be decreased, consistent with the above description. Thus, under the total internal reflection conditions, more trapped sky-blue photons from the p–i–n heterojunction can be more easily extracted out of the device through the thinner perovskite layer, which makes it possible to achieve a higher outcoupling efficiency in device W4.

**Table 1. Summary of the Device Performance of Perovskite/Organic Hybrid White LEDs**

device	$V_{\text{on}}$ (V)	$L_{\text{max}}$ ( $\text{cd m}^{-2}$ )	$\text{CE}_{\text{max}}$ ( $\text{cd A}^{-1}$ )	$\text{EQE}_{\text{max}}$ (%)	CCT (K)	CIE ( $x, y$ )
W1	2.9	227	3.45	5.46		(0.558, 0.330)
W2	3.1	148	5.13	6.16	2348	(0.456, 0.362)
W3	4.0	48	3.99	2.96	3862	(0.388, 0.367)
W4	3.0	764	7.62	7.35	2868	(0.424, 0.363)
W5	2.9	1162	7.35	5.54	4038	(0.377, 0.370)

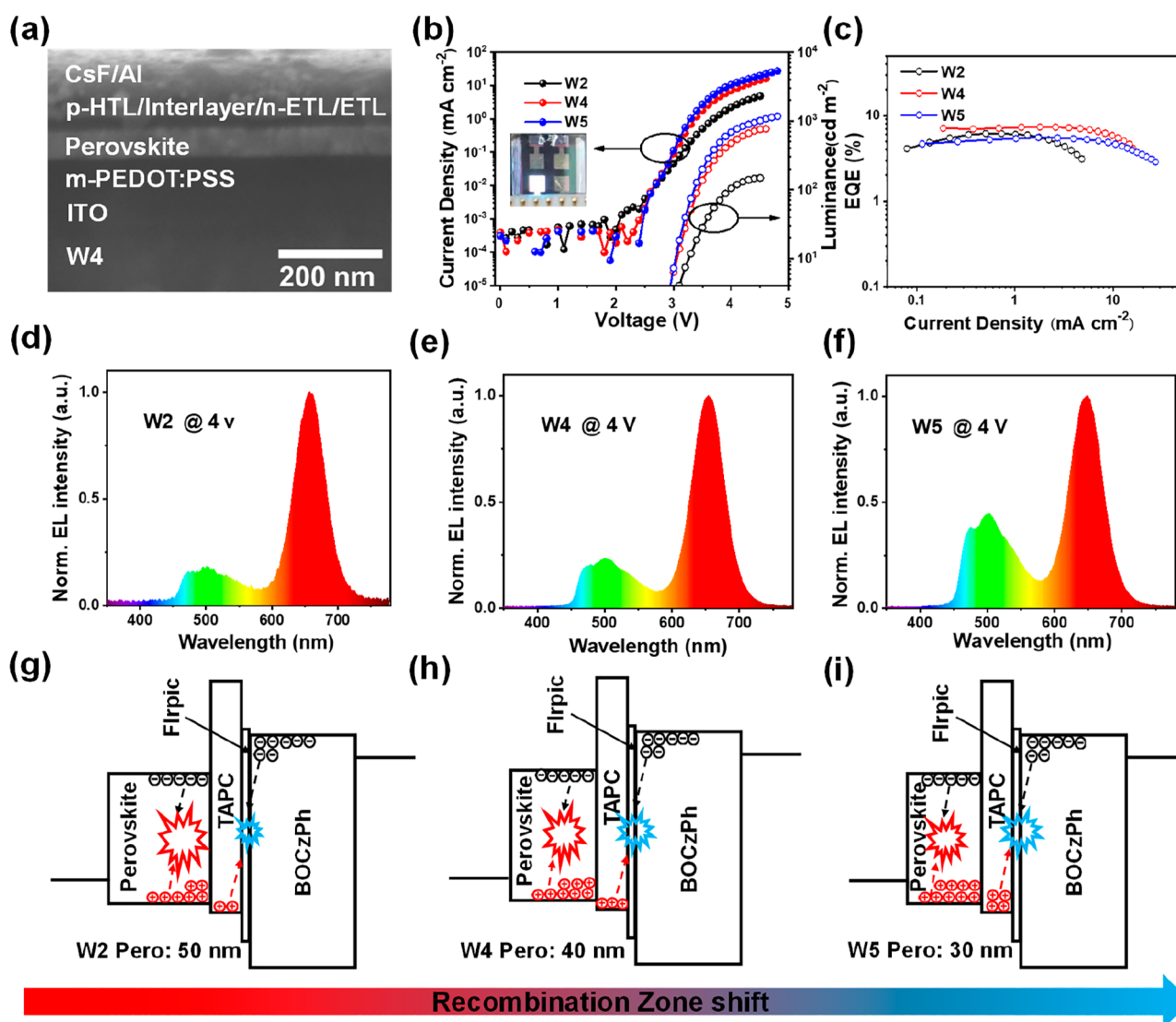
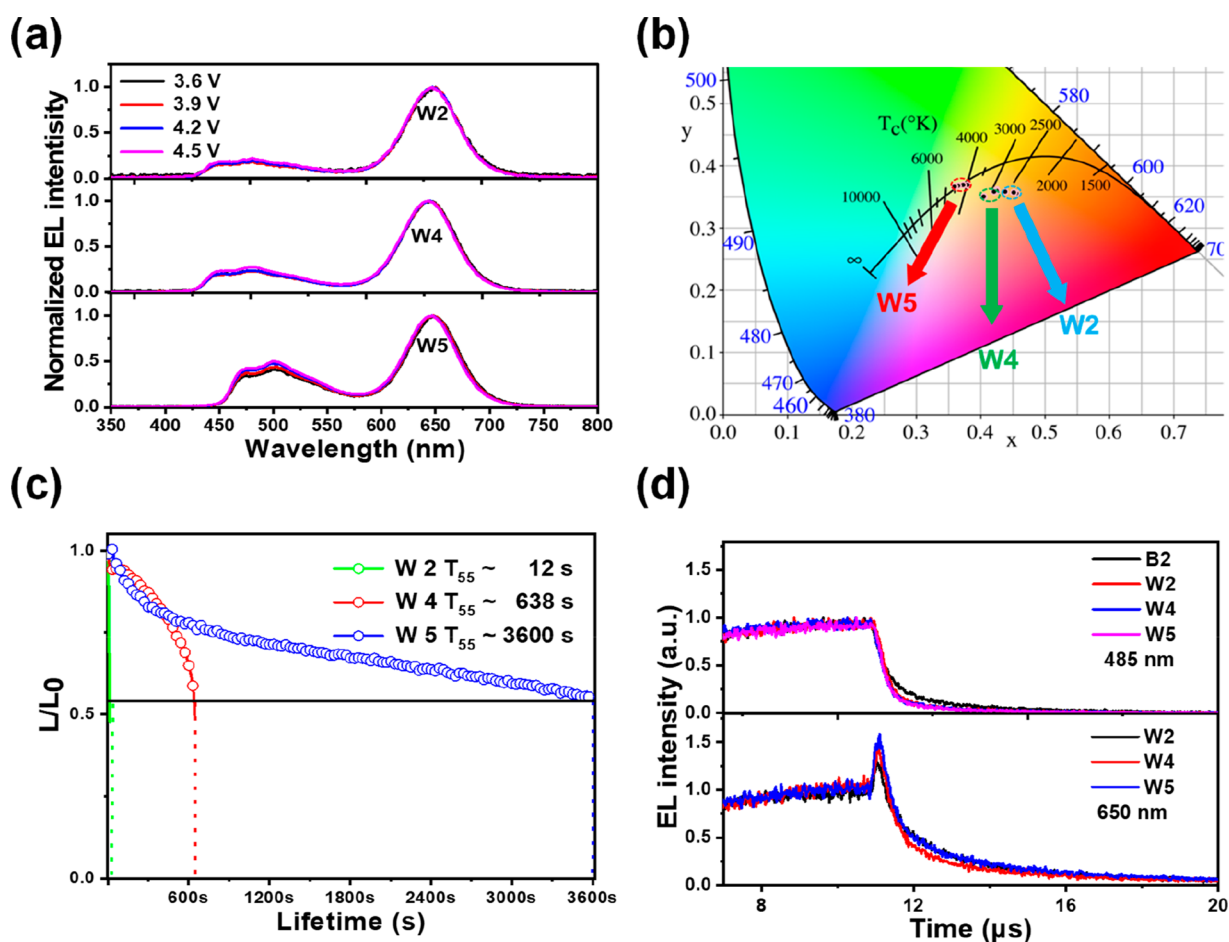


Figure 3. (a) Cross-sectional SEM image of device W4. (b)  $J$ - $V$ - $L$  (inset: photograph of working device W4) and (c) EQE- $J$  characteristics of devices W2, W4, and W5. EL spectra of devices (d) W2, (e) W4, and (f) W5 at 4 V. Schematic descriptions for the working mechanisms of devices (g) W2, (h) W4, and (i) W5.

The EL spectra of these devices exhibit tunable relative intensities of blue and red emissions (Figure 3d–f), corresponding to the change of CIE coordinates shown in Figure S19. Meanwhile, a small blue-shifted red emission peak was found for devices W4 and W5 in comparison with device W2, coinciding with their single-color EL devices (Figure S16a). The carrier injection was obviously enhanced (Figure 3b) due to the significantly enhanced hole transport ability with the decreasing thickness of the perovskite layer (Figure S15a). This further confirms that the perovskite layer participates in the process of electroluminescence instead of the excitation of the sky-blue emission p–i–n heterojunction, and the red component from the PL emission of the perovskite layer makes little contribution to the white emission (Note S7 and Figure S20 in the Supporting Information). For device W5, the peak EQE slightly decreases to 5.54% in spite of the maximum brightness climbing to  $1162 \text{ cd m}^{-2}$ . The higher trap density and much increased nonradiative recombination in the 30 nm perovskite film may account for the decreased EQE. On the basis of device W2, on solely decreasing the thickness of the perovskite layer to fabricate devices W4 and W5, the

thinner perovskite film with higher hole mobility will introduce more holes to be injected into the perovskite layer. However, the injected electrons within the perovskite layer still remain nearly unchanged at the same applied bias. In this case, more uncaptured holes from the perovskite layer will be allowed to pass through the TAPC layer and reach the organic p–i–n heterojunction for more blue emission. Thus, the recombination zone further shifts to the direction of the p–i–n heterojunction, as shown by the schematic descriptions in Figure 3g–i.

A steady white emission and a long operating lifespan are valuable for the practical application of illumination. Here, the EL spectral stabilities and operating lifetimes of devices W2, W4, and W5 are further investigated. Excitedly, these devices exhibit excellent EL stability with nearly no shift in CIE coordinates (Figure 4a,b) at different operating biases from 3.6 to 4.5 V, indicating that the position of the carrier recombination region is nearly unaffected by the driving voltages. This means that the hole transport controlled by the perovskite layer and the electron transport dominated by the tunneling effect of the TAPC layer increase simultaneously



**Figure 4.** (a) EL spectra and (b) corresponding CIE coordinates of devices W2, W4, and W5 at various driving voltages. (c) Operating lifetimes of devices W2, W4, and W5 measured at an initial brightness of  $100 \text{ cd m}^{-2}$  (driven at current densities of 3.8, 2.4, and  $1.8 \text{ mA cm}^{-2}$ , respectively). (d) Transient EL decay curves of devices B2, W2, W4, and W5 measured at 485 nm and of W2, W4, and W5 measured at 650 nm.

with increasing operating bias. Then, the operating stability of these devices was measured in an  $\text{N}_2$ -filled glovebox without encapsulation.  $T_{55}$  served as a unified standard to evaluate the operating lifetime of these white LEDs, which is defined by the time when the device brightness decreases to 55% of its initial brightness ( $L_0$ ). Here,  $L_0$  is set at around  $100 \text{ cd m}^{-2}$  and all devices are tested under a constant driving current. Interestingly, as shown in Figure 4c, in comparison to the operating lifespan of device W2 ( $T_{55} \approx 12 \text{ s}$ , measured @  $3.8 \text{ mA cm}^{-2}$ ), devices W4 ( $T_{55} \approx 638 \text{ s}$ , measured @  $2.4 \text{ mA cm}^{-2}$ ) and W5 ( $T_{55} \approx 3600 \text{ s}$ , measured @  $1.8 \text{ mA cm}^{-2}$ ) show substantially longer operating lifetimes. Furthermore, the lifetimes of their monochromatic pure-red perovskite LED (R1) and sky-blue p-i-n heterojunction organic LED (B2) are also measured for comparison, with corresponding operating lifespans of  $T_{55} \approx 60 \text{ s}$  (measured @  $4.6 \text{ mA cm}^{-2}$ ) and  $T_{55} \approx 228 \text{ s}$  (measured @  $0.8 \text{ mA cm}^{-2}$ ), respectively (Figure S21). When the operating stability was tested at the same initial brightness, note that with a greater contribution of the blue component to white emission, a lower driving current density close to that of device B2 was required. However, device W2 shows a poorer operating lifespan in comparison with device R1 (without using the organic p-i-n heterojunction) in spite of the lower current density applied. As was noted above, the electrons injected into the perovskite layer were controlled by the 5 nm TAPC layer. Considering

the lower hole mobility of the 50 nm perovskite layer, fewer holes can pass through the TAPC layer to encounter with extra excess electrons accumulated at the interface of the p-n heterojunction. This will lead to extremely unbalanced carrier recombination in the organic light-emitting unit, and it may be the main cause for the worse operating stability in device W2. Fortunately, significantly improved operating lifetimes are realized for devices W4 and W5 (for device W4, 10-fold longer than that for device R1, 2.7 times longer than that for device B2). Meanwhile, the operating lifetimes of the perovskite-only devices with 40 nm (device R2,  $T_{55} \approx 66 \text{ s}$ ) and 30 nm (device R3,  $T_{55} \approx 80 \text{ s}$ ) perovskite films as emitting layers were also measured for comparison (Figure S21), but no obvious extension of the operating lifetime was found in devices R2 and R3 in comparison with device R1, indicating the much enhanced lifetimes in devices W4 and W5 might not stem from the increased stability of the perovskite layer. In a word, this means that the extended device operating lifetime is inseparable from the aging of the p-i-n heterojunction. Thereby, in comparison with device W2, the following main reasons might account for the considerably extended operating lifetimes in devices W4 and W5. (i) The organic planar p-n heterojunction tends to have a faster aging rate, in which a high exciton concentration at the interface will aggravate triplet-triplet annihilation (TTA) and triplet-polaron annihilation (TPA) processes.<sup>35</sup> However, for devices W4 and W5, more



untrapped holes pass through the TAPC layer, facilitating a balance of the carrier recombination in the p–n heterojunction, together with a broadened recombination zone and partial electrons are transported to the perovskite layer via a tunneling effect, resulting in reduced exciton concentration at the interface of the p–n heterojunction and thus suppressed TTA and TPA processes. (ii) The possibility of exciton annihilation is highly related to the exciton lifetime of phosphorescence. Thus, the exciton dynamics in devices B2, W2, W4, and W5 were analyzed under electrical excitation via transient EL decay kinetics (Figure 4d). In comparison with device B2, devices W2, W4, and W5 exhibit relatively shorter exciton lifetimes at 485 nm, indicating that the ET process from the blue-emitting unit to the red perovskite layer is still inevitable. However, for the red perovskite layer, this sensitizing process can accelerate the exciton deactivation dynamics and shorten the lifetime of the excited state for the organic phosphorescent interlayer. It is necessary to emphasize that this process does not play a dominant role in device stability, for which device W2 with a decreased exciton lifetime still exhibits poorer device stability. (iii) As shown in Figure 4d, the EL dynamics of devices W2, W4, and W5 measured at 650 nm exhibit a more obvious overshoot effect in comparison to that detected at 485 nm, indicating a higher defect state density in the perovskite layer (Note S8 and Figure S22 in the Supporting Information). Thus, at the same initial luminance, the operating lifetimes of devices W4 and W5 are measured to have lower current density, leading to reduced nonradiative recombination in the perovskite layer, together with more trapped photons being extracted to decrease the local heat of the perovskite layer and thus inhibiting rapid decomposition of the perovskite. Consequently, the operating lifespan is improved for perovskite/organic hybrid white LEDs. This finding indicates that the presented device architectures show great potential for prolonging the lifespan of perovskite/organic hybrid white LEDs. As shown in Figure S23, with increasing working time, the normalized EL spectra of devices W2, W4, and W5 have stronger blue emission intensity, indicating that the aging of the perovskite/organic hybrid white LEDs still mainly comes from the decomposition of the perovskite. Thus, one should focus on an improvement in the stability of perovskite materials to further improve the operating stability of the perovskite/organic hybrid white LEDs.

In summary, we have successfully demonstrated a simple and convenient path to develop perovskite/organic hybrid white LEDs by combining a successively stacked pure-red perovskite and sky-blue organic p–i–n heterojunction as emissive layers. By a rational adjustment of the thickness of the p-HTL and perovskite layers to manage hole and electron transport properties in the device, the carrier recombination region can be effectively modulated, enabling a highly tunable white emission from pure-red perovskite and sky-blue organic phosphorescent emitters. Thanks to the suppressed ET process and higher exciton utilization in the presented device structure, a peak EQE of 7.35% and brightness of 746 cd m<sup>-2</sup> were achieved for the developed perovskite/organic hybrid white LEDs, with CIE coordinates of (0.424, 0.363) and a CCT value of 2868 K, which represents the state-of-the-art device performance in perovskite/organic hybrid white LEDs to date. Notably, these devices also exhibit stable EL spectra under various driving voltages and a greatly enhanced operating lifespan, which is especially important for their practical

application in solid-state lighting. We believe the presented device architecture will provide a workable idea for device design and pave the way for the development of high-performance perovskite/organic hybrid white LEDs.

## EXPERIMENTAL SECTION

**Materials.** Cesium iodide (CsI, 99.5%), methylamine iodide (MAI, 99.5%), lead iodide (PbI<sub>2</sub>, 99.5%), and phenethylamine iodide (PEAI, 99.5%) were purchased from Xi'an p-OLED Corp. Zinc iodide (ZnI<sub>2</sub>, 99.995%) was purchased from 3A Chemical Co., Ltd. Poly(sodium 4-styrenesulfonate) (PSS-Na, average  $M_w \approx 70000$ ), dimethylformamide (DMF, 99.8%), and dimethyl sulfoxide (DMSO, 99.7%) were purchased from Sigma-Aldrich (Shanghai) Trading Co., Ltd. PEDOT:PSS (AI 4083), TAPC, TPBI, and FIrpic were purchased from Luminescence Technology Corp. Aside from BOCzPh, which was synthesized by our group and further purified via vacuum sublimation (Supporting Information), the other materials were used as received without any further purification.

**Preparation of Quasi-2D Perovskite Films.** CsI was dissolved in DMSO (0.6 M), MAI, PbI<sub>2</sub>, ZnI<sub>2</sub>, and PEAi were dissolved in DMF (0.6 M), and they were stirred at 50 °C for 12 h in a nitrogen-filled glovebox. The (PEA)<sub>2</sub>(Cs<sub>0.3</sub>MA<sub>0.7</sub>)<sub>2</sub>(Pb<sub>0.7</sub>Zn<sub>0.3</sub>)<sub>3</sub>I<sub>10</sub> precursor solution was prepared by mixing CsI, MAI, PbI<sub>2</sub>, ZnI<sub>2</sub>, and PEAi in an appropriate molar ratio, and then the molar concentration of Pb<sup>2+</sup> plus Zn<sup>2+</sup> was adjusted to be 0.13 M. After 12 h, the 50 nm perovskite film was fabricated by spin-coating the prepared precursor solution at 4000 rpm for 40 s with the assistance of 100 μL of an antisolvent (chlorobenzene, 8 s). Perovskite films with thicknesses of 40 and 30 nm were prepared by diluting the molar concentrations of the perovskite precursor solution (Zn<sup>2+</sup> + Pb<sup>2+</sup>) to 0.10 and 0.07 M, respectively. The chemical formula and film formation method are consistent with the above description. m-PEDOT:PSS was prepared by mixing PEDOT:PSS (AI 4083) with PSS-Na (200 mg mL<sup>-1</sup>, dissolved in deionized water) at a volume ratio of 6:1.

**Characterizations of Perovskite and Organic Samples.** The top- and cross-sectional SEM images were obtained with a JEOL JSM-7500F system. The surface morphology images of perovskite films were obtained with an atomic force microscope (AFM) (Benyuan Corporation, BY3000). X-ray diffraction (XRD) spectra were obtained with a multipurpose Gemen Bruker D8 advance XRD system (Cu K $\alpha$ ,  $\lambda = 1.5406$  Å). PL spectra and UV–vis absorption spectra were measured by employing a Jobin–Yvon spectrofluorometer and a HP 8453 spectrophotometer, respectively. Transient PL decays were measured with an Edinburgh FL980 fluorescence spectrophotometer, equipped with an excitation light source (371.6 nm picosecond diode laser). The PLQYs of the perovskite films were recorded by a commercialized PLQY measurement system from Ocean Optics with excitation from a 365 nm LED. The ionization potential (IP) values of these perovskite films were measured by atmospheric ultraviolet photoelectron spectroscopy (Rikken Keiki AC-3). The current–voltage characteristics of the hole-only and electron-only devices were measured with a Keithley 2450 instrument controlled by Photo Research a PR745 system in a dark environment.

**Device Fabrication and Characterization.** With device W2 as an example, a perovskite/organic hybrid white LED was prepared with an architecture of ITO/m-PEDOT:PSS (30

nm)/perovskite (50 nm)/TAPC (5 nm)/Flrpic (1 nm)/BOCzPh (20 nm)/TPBI (30 nm)/CsF (1.2 nm)/Al (120 nm). m-PEDOT:PSS was spin-coated onto indium tin oxide (ITO, 95 nm) at 9000 rpm for 60 s and then backed at 160 °C for 15 min. After cooling, the perovskite films were prepared by spin-coating at 4000 rpm for 40 s with the assistance of 100 mL of chlorobenzene as an antisolvent (8 s) and then transferred to an evaporation chamber. After the vacuum was below  $3 \times 10^{-4}$  pa, TAPC, Flrpic, BOCzPh, TPBI, and the cathode (i.e., CsF and Al) were deposited layer by layer by thermal evaporation with a shadow mask to define an active area of 10 mm<sup>2</sup>; the thicknesses of various evaporated functional layers were monitored by a quartz crystal thickness monitor (SQC-310, Inficon). All preparation processes were carried out inside an N<sub>2</sub>-filled glovebox (oxygen, moisture <1 ppm). The optical parameters of *n* (refractive index) and *k* (extinction coefficient) for different films were measured using a dual rotating-compensator Mueller matrix ellipsometer (MEL ellipsometer, Wuhan Eoptics Technology, China). The EL spectra, *J*–*V*–*L* curves, EQE values, and operating lifespans of devices were collected by using the well-established system XPQY-eq E-350-1100 (Guangzhou Xi Pu Optoelectronics Technology Co., Ltd.), equipped with an integrating sphere (GPS-4P-SL, Labsphere) and a photodetector array (S7031-1006, Hamamatsu Photonics). The transient EL dynamics were measured with a digital oscilloscope (Tektronix, AFG3152C) to provide rectangular pulse voltages (repetition rate 20 kHz, width 10 μs) to drive the devices, and detected by an Edinburgh FL980 fluorescence spectrophotometer. Aside from the transient EL dynamics of devices that were measured in air (encapsulated with a UV-cured epoxy resin), the other characterizations of devices were carried out in an N<sub>2</sub>-filled glovebox without encapsulation.

## ■ ASSOCIATED CONTENT

### SI Supporting Information

The Supporting Information is available free of charge at <https://pubs.acs.org/doi/10.1021/acsenergylett.1c02631>.

Additional experimental procedures, characterizations, and discussions of the perovskite/organic hybrid white LEDs, summary of the optical properties of the perovskite films with different thicknesses, performance summary of devices R1–R3, B1–B3, and W6, and summary of the reported perovskite-based white electro-luminescent devices (PDF)

## ■ AUTHOR INFORMATION

### Corresponding Author

Shi-Jian Su – State Key Laboratory of Luminescent Materials and Devices and Institute of Polymer Optoelectronic Materials and Devices, South China University of Technology, Guangzhou 510640, People's Republic of China; [orcid.org/0000-0002-6545-9002](https://orcid.org/0000-0002-6545-9002); Email: [mssjsu@scut.edu.cn](mailto:mssjsu@scut.edu.cn)

### Authors

Denghui Liu – State Key Laboratory of Luminescent Materials and Devices and Institute of Polymer Optoelectronic Materials and Devices, South China University of Technology, Guangzhou 510640, People's Republic of China

Xinyan Liu – State Key Laboratory of Luminescent Materials and Devices and Institute of Polymer Optoelectronic Materials and Devices, South China University of Technology, Guangzhou 510640, People's Republic of China

Yiyang Gan – State Key Laboratory of Luminescent Materials and Devices and Institute of Polymer Optoelectronic Materials and Devices, South China University of Technology, Guangzhou 510640, People's Republic of China

Zhe Liu – State Key Laboratory of Luminescent Materials and Devices and Institute of Polymer Optoelectronic Materials and Devices, South China University of Technology, Guangzhou 510640, People's Republic of China

Guanwei Sun – State Key Laboratory of Luminescent Materials and Devices and Institute of Polymer Optoelectronic Materials and Devices, South China University of Technology, Guangzhou 510640, People's Republic of China

Chenyang Shen – State Key Laboratory of Luminescent Materials and Devices and Institute of Polymer Optoelectronic Materials and Devices, South China University of Technology, Guangzhou 510640, People's Republic of China

Xiaomei Peng – State Key Laboratory of Luminescent Materials and Devices and Institute of Polymer Optoelectronic Materials and Devices, South China University of Technology, Guangzhou 510640, People's Republic of China

Weidong Qiu – State Key Laboratory of Luminescent Materials and Devices and Institute of Polymer Optoelectronic Materials and Devices, South China University of Technology, Guangzhou 510640, People's Republic of China

Deli Li – State Key Laboratory of Luminescent Materials and Devices and Institute of Polymer Optoelectronic Materials and Devices, South China University of Technology, Guangzhou 510640, People's Republic of China

Zhisheng Zhou – State Key Laboratory of Luminescent Materials and Devices and Institute of Polymer Optoelectronic Materials and Devices, South China University of Technology, Guangzhou 510640, People's Republic of China

Zhenchao Li – State Key Laboratory of Luminescent Materials and Devices and Institute of Polymer Optoelectronic Materials and Devices, South China University of Technology, Guangzhou 510640, People's Republic of China

Hin-Lap Yip – State Key Laboratory of Luminescent Materials and Devices and Institute of Polymer Optoelectronic Materials and Devices, South China University of Technology, Guangzhou 510640, People's Republic of China; [orcid.org/0000-0002-5750-9751](https://orcid.org/0000-0002-5750-9751)

Complete contact information is available at: <https://pubs.acs.org/10.1021/acsenergylett.1c02631>

### Notes

The authors declare no competing financial interest.

## ■ ACKNOWLEDGMENTS

The authors greatly appreciate financial support from the National Natural Science Foundation of China (51625301, 91733302, and 51861145301), the Basic and Applied Basic Research Foundation of Guangdong Province



(2019B1515120023), the Guangdong Provincial Department of Science and Technology (2016B090906003 and 2016TX03C175), and the Dongguan Innovative Research Team Program (2018607201002).

## REFERENCES

- (1) Stranks, S. D.; Snaith, H. J. Metal-halide Perovskites for Photovoltaic and Light-Emitting Devices. *Nat. Nanotechnol.* **2015**, *10* (5), 391–402.
- (2) Cho, H.; Jeong, S. H.; Park, M. H.; Kim, Y. H.; Wolf, C.; Lee, C. L.; Heo, J. H.; Sadhanala, A.; Myoung, N.; Yoo, S.; Im, S. H.; Friend, R. H.; Lee, T. W. Overcoming the Electroluminescence Efficiency Limitations of Perovskite Light-Emitting Diodes. *Science* **2015**, *350* (6265), 1222–1225.
- (3) Meng, F.; Liu, X.; Chen, Y.; Cai, X.; Li, M.; Shi, T.; Chen, Z.; Chen, D.; Yip, H. L.; Ramanan, C.; Blom, P. W. M.; Su, S.-J. Co-Interlayer Engineering toward Efficient Green Quasi-Two-Dimensional Perovskite Light-Emitting Diodes. *Adv. Funct. Mater.* **2020**, *30* (19), 1910167.
- (4) Liu, X. K.; Xu, W.; Bai, S.; Jin, Y.; Wang, J.; Friend, R. H.; Gao, F. Metal Halide Perovskites for Light-Emitting Diodes. *Nat. Mater.* **2021**, *20* (1), 10–21.
- (5) Savenije, T. J.; Ponseca, C. S.; Kunneman, L.; Abdellah, M.; Zheng, K. B.; Tian, Y. X.; Zhu, Q. S.; Canton, S. E.; Scheblykin, I. G.; Pullerits, T.; Yartsev, A.; Sundstrom, V. Thermally Activated Exciton Dissociation and Recombination Control the Carrier Dynamics in Organometal Halide Perovskite. *J. Phys. Chem. Lett.* **2014**, *5* (13), 2189–2194.
- (6) Kim, Y.-H.; Kim, S.; Kakekhani, A.; Park, J.; Park, J.; Lee, Y.-H.; Xu, H.; Nagane, S.; Wexler, R. B.; Kim, D.-H.; Jo, S. H.; Martínez-Sarti, L.; Tan, P.; Sadhanala, A.; Park, G.-S.; Kim, Y.-W.; Hu, B.; Bolink, H. J.; Yoo, S.; Friend, R. H.; Rappe, A. M.; Lee, T.-W. Comprehensive Defect Suppression in Perovskite Nanocrystals for High-Efficiency Light-Emitting Diodes. *Nat. Photonics* **2021**, *15* (2), 148–155.
- (7) Chu, Z.; Ye, Q.; Zhao, Y.; Ma, F.; Yin, Z.; Zhang, X.; You, J. Perovskite Light-Emitting Diodes with External Quantum Efficiency Exceeding 22% via Small-Molecule Passivation. *Adv. Mater.* **2021**, *33* (18), 2007169–2007178.
- (8) Chiba, T.; Hayashi, Y.; Ebe, H.; Hoshi, K.; Sato, J.; Sato, S.; Pu, Y. J.; Ohisa, S.; Kido, J. Anion-Exchange Red Perovskite Quantum Dots with Ammonium Iodine Salts for Highly Efficient Light-Emitting Devices. *Nat. Photon.* **2018**, *12* (11), 681–687.
- (9) Cao, Y.; Wang, N.; Tian, H.; Guo, J.; Wei, Y.; Chen, H.; Miao, Y.; Zou, W.; Pan, K.; He, Y.; Cao, H.; Ke, Y.; Xu, M.; Wang, Y.; Yang, M.; Du, K.; Fu, Z.; Kong, D.; Dai, D.; Jin, Y.; Li, G.; Li, H.; Peng, Q.; Wang, J.; Huang, W. Perovskite Light-Emitting Diodes Based on Spontaneously Formed Submicrometre-Scale Structures. *Nature* **2018**, *562* (7726), 249–253.
- (10) Zhu, Z.; Wu, Y.; Shen, Y.; Tan, J.; Shen, D.; Lo, M.-F.; Li, M.; Yuan, Y.; Tang, J.-X.; Zhang, W.; Tsang, S.-W.; Guan, Z.; Lee, C.-S. Highly Efficient Sky-Blue Perovskite Light-Emitting Diode Via Suppressing Nonradiative Energy Loss. *Chem. Mater.* **2021**, *33* (11), 4154–4162.
- (11) Dong, Y.; Wang, Y.-K.; Yuan, F.; Johnston, A.; Liu, Y.; Ma, D.; Choi, M.-J.; Chen, B.; Chekini, M.; Baek, S.-W.; Sagar, L. K.; Fan, J.; Hou, Y.; Wu, M.; Lee, S.; Sun, B.; Hoogland, S.; Quintero-Bermudez, R.; Ebe, H.; Todorovic, P.; Dinic, F.; Li, P.; Kung, H. T.; Saidaminov, M. I.; Kumacheva, E.; Spiecker, E.; Liao, L.-S.; Voznyy, O.; Lu, Z.-H.; Sargent, E. H. Bipolar-Shell Resurfacing for Blue LEDs Based on Strongly Confined Perovskite Quantum Dots. *Nat. Nanotechnol.* **2020**, *15*, 668–674.
- (12) Chu, Z.; Zhao, Y.; Ma, F.; Zhang, C. X.; Deng, H.; Gao, F.; Ye, Q.; Meng, J.; Yin, Z.; Zhang, X.; You, J. Large Cation Ethylammonium Incorporated Perovskite for Efficient and Spectra Stable Blue Light-Emitting Diodes. *Nat. Commun.* **2020**, *11* (1), 4165–4173.
- (13) Huang, C.-Y.; Huang, S.-J.; Liu, M.-H. M. Hybridization of CsPbBr<sub>1.5</sub>I<sub>1.5</sub> Perovskite Quantum Dots with 9,9-dihexylfluorene Co-Oligomer for White Electroluminescence. *Org. Electron.* **2017**, *44*, 6–10.
- (14) Sun, C.; Zhang, Y.; Ruan, C.; Yin, C. Y.; Wang, X. Y.; Wang, Y. D.; Yu, W. W. Efficient and Stable White LEDs with Silica-Coated Inorganic Perovskite Quantum Dots. *Adv. Mater.* **2016**, *28* (45), 10088–10094.
- (15) Mao, J.; Lin, H.; Ye, F.; Qin, M.; Burkhartsmeyer, J. M.; Zhang, H.; Lu, X.; Wong, K. S.; Choy, W. C. H. All-Perovskite Emission Architecture for White Light-Emitting Diodes. *ACS Nano* **2018**, *12* (10), 10486–10492.
- (16) Chang, C.-Y.; Solodukhin, A. N.; Liao, S.-Y.; Mahesh, K. P. O.; Hsu, C.-L.; Ponomarenko, S. A.; Luponosov, Y. N.; Chao, Y.-C. Perovskite White Light-Emitting Diodes Based on a Molecular Blend Perovskite Emissive Layer. *J. Mater. Chem. C* **2019**, *7* (28), 8634–8642.
- (17) Wang, C.; Xue, D.; Shen, X.; Wu, H.; Zhang, Y.; Cui, H.; Yu, W. W. White Light-Emitting Devices Based on ZnCdS/ZnS and Perovskite Nanocrystal Heterojunction. *Nanotechnol.* **2019**, *30* (46), 465201–465209.
- (18) Chen, S. M.; Chen, C.; Bao, C.; Mujahid, M.; Li, Y.; Chen, P.; Duan, Y. White Light-Emitting Devices Based on Inorganic Perovskite and Organic Materials. *Molecules* **2019**, *24*, 800.
- (19) Jamaludin, N. F.; Yantara, N.; Giovanni, D.; Febriansyah, B.; Tay, Y. B.; Salim, T.; Sum, T. C.; Mhaisalkar, S.; Mathews, N. White Electroluminescence from Perovskite–Organic Heterojunction. *ACS Energy Lett.* **2020**, *5* (8), 2690–2697.
- (20) Sun, R.; Lu, P.; Zhou, D.; Xu, W.; Ding, N.; Shao, H.; Zhang, Y.; Li, D.; Wang, N.; Zhuang, X.; Dong, B.; Bai, X.; Song, H. Samarium-Doped Metal Halide Perovskite Nanocrystals for Single-Component Electroluminescent White Light-Emitting Diodes. *ACS Energy Lett.* **2020**, *5* (7), 2131–2139.
- (21) Chang, C.-Y.; Hong, W.-L.; Lo, P.-H.; Wen, T.-H.; Horng, S.-F.; Hsu, C.-L.; Chao, Y.-C. Perovskite White Light-Emitting Diodes with a Perovskite Emissive Layer Blended with Rhodamine 6G. *J. Mater. Chem. C* **2020**, *8* (37), 12951–12958.
- (22) Yu, H.; Wang, H.; Pozina, G.; Yin, C.; Liu, X.-K.; Gao, F. Single-Emissive-Layer All-Perovskite White Light-Emitting Diodes Employing Segregated Mixed Halide Perovskite Crystals. *Chem. Sci.* **2020**, *11* (41), 11338–11343.
- (23) Chen, H.; Zhu, L.; Xue, C.; Liu, P.; Du, X.; Wen, K.; Zhang, H.; Xu, L.; Xiang, C.; Lin, C.; Qin, M.; Zhang, J.; Jiang, T.; Yi, C.; Cheng, L.; Zhang, C.; Yang, P.; Niu, M.; Xu, W.; Lai, J.; Cao, Y.; Chang, J.; Tian, H.; Jin, Y.; Lu, X.; Jiang, L.; Wang, N.; Huang, W.; Wang, J. Efficient and Bright Warm-White Electroluminescence from Lead-Free Metal Halides. *Nat. Commun.* **2021**, *12* (1), 1421–1427.
- (24) Chen, J.; Wang, J.; Xu, X.; Li, J.; Song, J.; Lan, S.; Liu, S.; Cai, B.; Han, B.; Precht, J. T.; Ginger, D.; Zeng, H. Efficient and Bright White Light-Emitting Diodes Based on Single-Layer Heterophase Halide Perovskites. *Nat. photon.* **2021**, *15*, 238–244.
- (25) Yao, E. P.; Yang, Z. L.; Meng, L.; Sun, P. Y.; Dong, S. Q.; Yang, Y.; Yang, Y. High-Brightness Blue and White LEDs Based on Inorganic Perovskite Nanocrystals and their Composites. *Adv. Mater.* **2017**, *29* (23), 1606859.
- (26) Jun, T.; Sim, K.; Iimura, S.; Sasase, M.; Kamioka, H.; Kim, J.; Hosono, H. Lead-Free Highly Efficient Blue-Emitting Cs<sub>3</sub>Cu<sub>2</sub>I<sub>5</sub> with 0D Electronic Structure. *Adv. Mater.* **2018**, *30*, 1804547.
- (27) Luo, J.; Wang, X.; Li, S.; Liu, J.; Guo, Y.; Niu, G.; Yao, L.; Fu, Y.; Gao, L.; Dong, Q.; Zhao, C.; Leng, M.; Ma, F.; Liang, W.; Wang, L.; Jin, S.; Han, J.; Zhang, L.; Etheridge, J.; Wang, J.; Yan, Y.; Sargent, E. H.; Tang, J. Efficient and Stable Emission of Warm-White Light from Lead-Free Halide Double Perovskites. *Nature* **2018**, *563*, 541–545.
- (28) Chi, Y.; Chou, P. T. Transition-Metal Phosphors with Cyclometalating Ligands: Fundamentals and Applications. *Chem. Soc. Rev.* **2010**, *39* (2), 638–655.
- (29) Karthik, D.; Jung, Y. H.; Lee, H.; Hwang, S.; Seo, B. M.; Kim, J. Y.; Han, C. W.; Kwon, J. H. Acceptor–Donor–Acceptor-Type Orange–Red Thermally Activated Delayed Fluorescence Materials

Realizing External Quantum Efficiency Over 30% with Low Efficiency Roll-Off. *Adv. Mater.* **2021**, *33*, 2007724.

(30) Chen, D.; Liu, K.; Gan, L.; Liu, M.; Gao, K.; Xie, G.; Ma, Y.; Cao, Y.; Su, S.-J. Modulation of Exciton Generation in Organic Active Planar pn Heterojunction: Toward Low Driving Voltage and High-Efficiency OLEDs Employing Conventional and Thermally Activated Delayed Fluorescent Emitters. *Adv. Mater.* **2016**, *28* (31), 6758–6765.

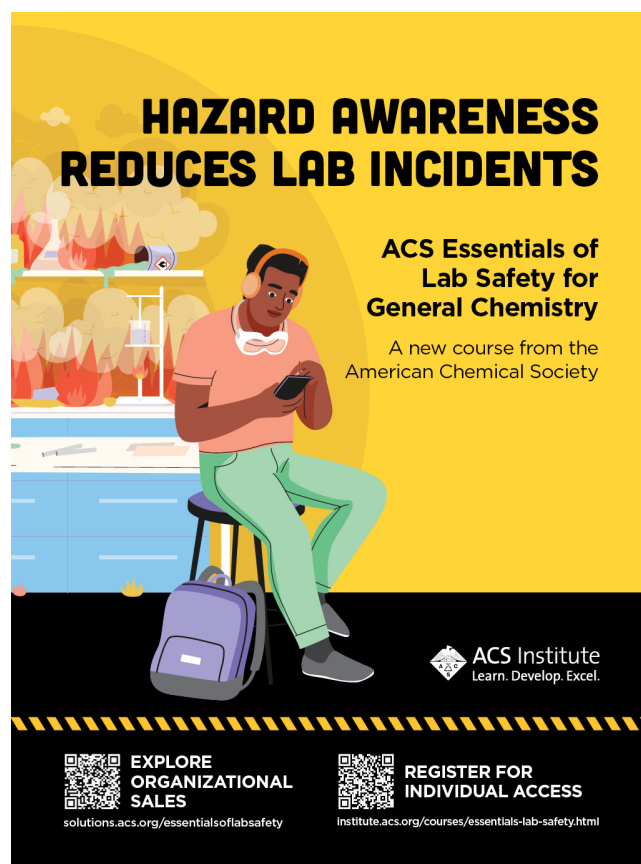
(31) Chen, D.; Xie, G.; Cai, X.; Liu, M.; Cao, Y.; Su, S.-J. Fluorescent Organic Planar pn Heterojunction Light-Emitting Diodes with Simplified Structure, Extremely Low Driving Voltage, and High Efficiency. *Adv. Mater.* **2016**, *28*, 239–244.

(32) Chen, D.; Li, B.; Gan, L.; Cai, X.; Ma, Y.; Cao, Y.; Su, S.-J. Enhanced Performances of Planar Heterojunction Organic Light-Emitting Diodes via Diluting an n-Type Transporter into a Carbazole-Based Matrix. *J. Mater. Chem. C* **2018**, *6* (1), 29–35.

(33) Li, B.; Gan, L.; Cai, X.; Li, X.; Wang, Z.; Gao, K.; Chen, D.; Cao, Y.; Su, S.-J. An Effective Strategy toward High-Efficiency Fluorescent OLEDs by Radiative Coupling of Spatially Separated Electron–Hole Pairs. *Adv. Mater. Interfaces* **2018**, *5* (10), 1800025.

(34) Zhang, M.; Zheng, C.-J.; Lin, H.; Tao, S.-L. Thermally Activated Delayed Fluorescence Exciplex Emitters for High-Performance Organic Light-Emitting Diodes. *Mater. Horiz.* **2021**, *8* (2), 401.

(35) Wang, Z.; Li, M.; Gan, L.; Cai, X.; Li, B.; Chen, D.; Su, S.-J. Predicting Operational Stability for Organic Light-Emitting Diodes with Exciplex Cohosts. *Adv. Sci.* **2019**, *6* (7), 1802246.



**HAZARD AWARENESS  
REDUCES LAB INCIDENTS**

**ACS Essentials of  
Lab Safety for  
General Chemistry**

A new course from the  
American Chemical Society

ACS Institute  
Learn. Develop. Excel.

EXPLORE  
ORGANIZATIONAL  
SALES  
[solutions.acs.org/essentialsoflabsafety](https://solutions.acs.org/essentialsoflabsafety)

REGISTER FOR  
INDIVIDUAL ACCESS  
[institute.acs.org/courses/essentials-lab-safety.html](https://institute.acs.org/courses/essentials-lab-safety.html)